Title

Multiantigenic Nanotoxoids for Antivirulence Vaccination against Antibiotic-Resistant Gram-Negative Bacteria

Journal

Nano Letters, 19(7)

ISSN

1530-6984

Authors

Wei, Xiaoli
Ran, Danni
Campeau, Anaamika
et al.

Publication Date

2019-07-10

DOI

10.1021/acs.nanolett.9b01844

Peer reviewed

HHS Public Access

Author manuscript

Nano Lett. Author manuscript; available in PMC 2020 July 10.

Published in final edited form as:

Nano Lett. 2019 July 10; 19(7): 4760–4769. doi:10.1021/acs.nanolett.9b01844.

Multiantigenic Nanotoxoids for Antivirulence Vaccination against Antibiotic-Resistant Gram-Negative Bacteria

Xiaoli Wei[†,‡,‖], **Danni Ran**[†,‡,‖], **Anaamika Campeau**[§], **Crystal Xiao**[†,‡], **Jiarong Zhou**[†,‡], **Diana Dehaini**[†,‡], **Yao Jiang**[†,‡], **Ashley V. Kroll**[†,‡], **Qiangzhe Zhang**[†,‡], **Weiwei Gao**[†,‡], **David J. Gonzalez**[§], **Ronnie H. Fang**[†,‡,*], **Liangfang Zhang**[†,‡,*]

[†]Department of NanoEngineering and Chemical Engineering Program, University of California San Diego, La Jolla, CA 92093

[‡]Moores Cancer Center, University of California San Diego, La Jolla, CA 92093

[§]Department of Pharmacology, Skaggs School of Pharmacy and Pharmaceutical Sciences, University of California San Diego, La Jolla, CA 92093

Abstract

Infections caused by multidrug-resistant gram-negative bacteria have emerged as a major threat to public health worldwide. The high mortality and prevalence, along with the slow pace of new antibiotic discovery, highlight the necessity for new disease management paradigms. Here, we report on the development of a multiantigenic nanotoxoid vaccine based on macrophage membrane-coated nanoparticles for eliciting potent immunity against pathogenic *Pseudomonas aeruginosa*. The design of this biomimetic nanovaccine leverages the specific role of macrophages in clearing pathogens and their natural affinity for various virulence factors secreted by the bacteria. It is demonstrated that the macrophage nanotoxoid is able to display a wide range of *P. aeruginosa* antigens, and the safety of the formulation is confirmed both *in vitro* and *in vivo*. When used to vaccinate mice via different administration routes, the nanotoxoid is capable of eliciting strong humoral immune responses that translate into enhanced protection against live bacterial infection in a pneumonia model. Overall, the work presented here provides new insights into the design of safe, multiantigenic antivirulence vaccines using biomimetic nanotechnology and the application of these nanovaccines towards the prevention of difficult-to-treat gram-negative infections.

Graphical Abstract

[*]Corresponding authors: rhfang@ucsd.edu (Tel: 858-246-2773) and zhang@ucsd.edu (Tel: 858-246-0999).
[‖]These authors contributed equally to this work.

Supporting Information

The Supporting Information is available free of charge on the ACS Publications website at DOI: 10.1021/acs.nano-lett.xrefX.

The authors declare no competing financial interest.

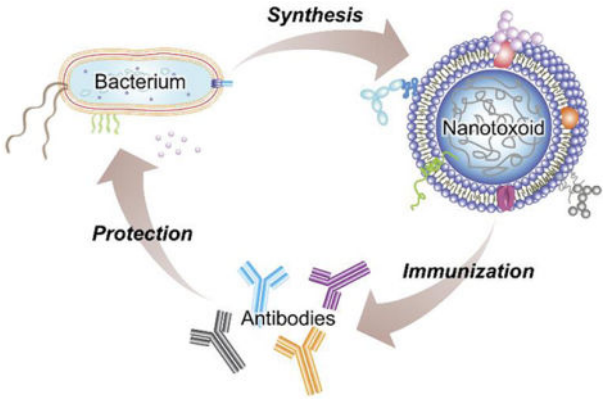

Keywords

biomimetic nanotechnology; antivirulence vaccination; nanotoxoid; gram-negative infection; *Pseudomonas aeruginosa*

The global incidence of infections caused by multidrug-resistant gram-negative bacteria has been increasing,[1] and this poses a major threat to public health given the high morbidity and mortality rates associated with these diseases.[2] *Pseudomonas aeruginosa* is one of the leading gram-negative bacteria responsible for life-threatening pneumonia, especially among the immunocompromised and among cystic fibrosis patients.[3] The pathogen has the ability to rapidly develop antibiotic resistance by different mechanisms, including the use of efflux pumps, expression of β-lactamase, reduction in porins, and switching to a biofilm lifestyle, among others.[4–6] This complicates the management of *P. aeruginosa* infections and contributes significantly to the suboptimal outcomes observed in the clinic.[4] The seriousness and increasing prevalence of multidrug-resistant *P. aeruginosa* has resulted in the World Health Organization declaring the pathogen a top priority.[7] Overall, the slow development of new antibiotics has presented a major challenge in the collective response against drug-resistant infections, leading researchers to actively seek new approaches for antibacterial therapy.[8–9]

Vaccines aim to prevent infectious diseases by training the immune system to recognize pathogen-associated antigenic targets.[10–11] Various formulations targeting *P. aeruginosa* antigens have been reported, including those designed to generate immunity against lipopolysaccharide O antigen, flagella, outer membrane proteins, and type III secretion system proteins.[12–13] While much progress has been made in recent years towards the development of effective *P. aeruginosa* vaccines, to date no such formulation has been licensed for clinical use. Virulence mechanisms are particularly attractive targets for vaccine development, as they are directly involved in host interactions that promote bacterial survival and proliferation.[14–15] Because there is no selection pressure imposed upon individual bacterium, antivirulence vaccination can also carry a lower risk of developing resistance.[16–17] The multifactorial virulence exhibited by *P. aeruginosa*, which includes various biomolecular secretions that can attack host cells,[18–19] represents a major challenge that naturally limits the effectiveness of any single-antigen antivirulence strategy being evaluated

for clinical application.[20] Developing multiantigenic vaccines, however, is not a straightforward process, particularly given that the identity, function, and safety profile of many bacterial components are still in the process of being elucidated.[21]

Recently, cell membrane-coated nanoparticles have emerged as a platform that has broad applicability.[22–23] Using naturally derived cell membrane as a surface coating, nanoparticles with cell-mimicking and biointerfacing functionalities can be readily fabricated.[24–28] These nanoparticles have been utilized as nanosponges that leverage the natural affinity of biological toxins for cell membrane to achieve broad-spectrum biodetoxification.[29–30] Taking advantage of the fact that bacterial toxins become deactivated upon complexation with nanosponges, the resulting nanoparticle–toxin constructs have been employed as nanotoxoids for use in antivirulence vaccination applications.[31] This approach has previously proven to be effective for gram-positive bacteria, eliciting immunity capable of preventing toxin-mediated damage and inhibiting bacteria colonization in murine models of disease.[32] Notably, a multiantigenic formulation fabricated from the combination of red blood cell (RBC) membrane-coated nanoparticles and *Staphylococcus aureus* protein secretions has been used to successfully elicit immunity against multiple virulence factors at the same time.[33]

Macrophages can act as a nonspecific second line of immune defense against bacterial infections.[34–35] *P. aeruginosa* interacts with macrophages in a number of ways that are not applicable to RBCs, including via non-hemolytic virulence factors, as well as through engagement of surface markers including toll-like receptors (TLRs) and phagocytosis-promoting receptors.[3] Cationic proteins on alveolar macrophages can bind avidly to the outer membrane of *P. aeruginosa*,[36] and the bacteria's flagella are involved in the phagocytic process.[37] *P. aeruginosa* also secrets several types of cytolysins that are toxic to macrophages and help the bacteria to colonize their hosts.[38] Taking advantage of these naturally occurring cell–bacterium interactions, macrophage membrane-coated nanoparticles (MΦ-NPs) have demonstrated the ability to bind and neutralize gram-negative bacterial toxins.[28] Compelled by the diverse interactions of macrophages with *P. aeruginosa*, here we employ MΦ-NPs to generate a multiantigenic macrophage nanotoxoid (MΦ-toxoid) against the bacteria (Figure 1). The MΦ-toxoids are fabricated by leveraging the broad-spectrum binding capabilities of cell membrane-coated nanoparticles, and the ability of the vaccine formulation to elicit potent immunity against *P. aeruginosa* is studied in detail.

To generate the MΦ-toxoid formulation, MΦ-NPs were first fabricated by a previously reported method.[28] Briefly, macrophage membrane was derived from a representative murine J774 cell line using a process involving mechanical disruption followed by differential centrifugation. The macrophage membrane was then coated onto preformed poly(lactic-*co*-glycolic acid) (PLGA) cores at a membrane protein to polymer weight ratio of 1:1 by sonication. Next, *P. aeruginosa* secretions (PaS) were collected from bacterial culture supernatant by ammonium sulfate precipitation as previously described.[33] The concentrated PaS was then subjected to size exclusion chromatography, and two resultant fractions, denoted PaS-1 and PaS-2, were identified and collected.

The PaS-1 fraction was shown to be hemolytic in a concentration-dependent manner (Figure 2a). Under the experimental conditions that were employed, 200 μg/mL of PaS-1 induced complete hemolysis of mouse RBCs, while minimal hemolysis was observed when the concentration was decreased to 100 μg/mL. Upon preincubation with MΦ-NPs at a 1:5 (PaS-1:MΦ-NP) protein ratio, the hemolytic activity of the fraction was completely abrogated. PaS-1 also exhibited a certain degree of cytotoxic activity upon incubation with J774 mouse macrophages in culture, with approximately 50% cell viability observed when incubating with 40 μg/mL of PaS-1 (Figure 2b). Again, the toxic effect was completely neutralized when preincubating with MΦ-NP at a 1:5 protein ratio. In contrast, PaS-2 did not show any hemolytic activity at high concentrations (Figure 2c), but it was cytotoxic even in small amounts (Figure 2d). After incubation with 4 μg/mL of PaS-2, no cell survival was observed in J774 cultures. When preincubating with MΦ-NPs at a 1:50 (PaS-2:MΦ-NP) protein ratio, approximately 30% cell viability was recovered. The benefit was more pronounced at a 1:200 protein ratio, where near full viability was achieved when including the nanoparticles, compared with 30% viability when incubating with PaS-2 alone at 1 μg/mL. For subsequent study, the final MΦ-toxoid was formulated by incubating 200 μg of MΦ-NPs with 40 μg of PaS-1 and 1 μg of PaS-2 in order to achieve the maximal antigen loading while maintaining safety. After coincubation of all the components, it was demonstrated that the MΦ-toxoids exhibited a slight size increase in comparison to unloaded MΦ-NPs, and the zeta potential became slightly more negative (Figure 2e,f). Transmission electron microscopy of the MΦ-toxoids negatively stained with uranyl acetate revealed that the characteristic core–shell structure of membrane-coated nanoparticles was retained after PaS loading (Figure 2g), which is consistent with previous reports on similar nanotoxoid formulations.[31] In terms of their stability in solution, the MΦ-toxoids did not change significantly in size over the course of 1 week (Figure 2h).

One of the main advantages of the cell membrane-based nanotoxoid strategy is that it enables the capture of a wide range of pathogen-specific antigens of unknown composition. It has been demonstrated that the binding of virulence factors to biomimetic membrane-coated nanoparticles varies depending on the cell type used to source the membrane.[39] In order to validate the presence of *P. aeruginosa*-specific proteins on the MΦ-toxoids, the formulation was characterized by a previously described multiplexed quantitative proteomic approach.[39] In total, 4,931 proteins were quantified on the MΦ-toxoid formulation, among which 4,792 were of mouse origin and 139 were of *P. aeruginosa* origin (Supplementary Table 1). Of the *P. aeruginosa* proteins that were quantified, 44 of these exhibited statistically significant enrichment on the MΦ-toxoids when assessed by π score ($\pi > 1.1082$, Figure 2i).[40] After analyzing the individual data points, there were some notable proteins that exhibited particularly high enrichment ratios (Figure 2j). Flagellin, which plays a critical role in the initial colonization phase of infection and serves as a ligand that enhances phagocytosis,[41] was enriched by 4.9-fold. Vaccine formulations targeting flagellin have been shown to confer protection against different strains of *P. aeruginosa* in mouse models of pneumonia by eliciting effective cellular and humoral immune responses.[42] The conserved domains of flagellin also serve as a pathogen-associated molecular pattern that is capable of inducing strong inflammatory responses *via* engagement of TLR5.[43] Additionally, the outer membrane proteins OprE and OprM were enriched by 3.1-fold and 4.5-fold, respectively.

Vaccines against *P. aeruginosa* outer membrane proteins have been reported to successfully confer protection against infection in mouse models.[44] Overall, the proteomic data validated the loading of multiple antigens relevant to vaccination against *P. aeruginosa*, which combined could work together to confer broader protection against the pathogen. It is notable that the fabrication process of MΦ-toxoids was carried out without the need for prior identification of each individual antigenic target.

Given the established toxicities of both the PaS-1 and PaS-2 fractions that were loaded onto the MΦ-toxoids, we next carried out a series of studies to establish the safety profile of the optimized vaccine formulation. A consolidated PaS-1/2 fraction was made by combining PaS-1 with PaS-2 at a protein ratio of 40:1 and subsequently incubated with either mouse RBCs or J774 cells *in vitro*. Native PaS-1/2 lysed 100% of the RBCs under the conditions tested, while the MΦ-toxoids induced a minimal amount of hemolysis that was near identical to unloaded MΦ-NPs (Figure 3a). As expected, PaS-1/2 was also highly cytotoxic to J774 cells, resulting in complete killing after 72 h of coincubation (Figure 3b). In contrast, there were minimal signs of cytotoxicity in cells incubated with the MΦ-toxoids, and the effect was statistically insignificant compared with unloaded MΦ-NPs. Next, *in vivo* safety was evaluated by administering the various formulations subcutaneously into mice, followed by histological analysis of the skin at the injection site after 48 h (Figure 3c). Hematoxylin and eosin (H&E) staining showed that native PaS-1/2 induced severe hyperplasia, parakeratosis, and ulceration in the epidermis, as well as fibrosis and bleeding in the dermis. There were no obvious signs of damage in the histological sections from mice administered with blank solution, unloaded MΦ-NPs, or MΦ-toxoids. In these samples, the structure of the skin remained intact. While only resident immune cell populations were present in the dermis for the blank solution and MΦ-NP groups, there was mild to moderate inflammatory infiltrate in the dermis and hypodermis for the MΦ-toxoid group. This was a positive observation that indicated the process of adaptive immunity had potentially been initiated in response to MΦ-toxoid administration.

After establishing the safety of the formulation, the ability of the MΦ-toxoid vaccine to elicit humoral immunity by different administration routes was evaluated. First, the generation of systemic immunity after subcutaneous vaccination was studied. As demonstrated previously, nanoparticle administration by this route leads to lymphatic drainage and uptake predominantly by antigen-presenting cells, including B cells.[45] The induction of germinal centers within the lymph nodes is a critical step in the humoral immune response that promotes the affinity-based maturation of B cells specialized in producing antibodies that can effectively recognize infectious agents,[46] and it should be noted that this occurs in concert with T cell-based immune mechanisms.[47–48] To explore the impact of our nanoformulation on this process, nearby lymph nodes, including the superficial cervical lymph node and axillary lymph node, were collected 21 days after immunization in the neck region and analyzed for the presence of germinal center B cells. Flow cytometric analysis revealed that the MΦ-toxoids could significantly raise the percentage of $B220^{+}IgD^{low}$ B cells with the $GL\text{-}7^{+}$ germinal center phenotype in the superficial cervical lymph node, with the value increasing to 45% compared with approximately 20% after vaccination with blank solution or unloaded MΦ-NPs (Figure 4a). This was also confirmed by immunofluorescence staining, as histological sections of the lymph nodes from MΦ-toxoid-vaccinated mice

displayed nodules with a high concentration of GL-7$^+$ cells, whereas those from mice treated with blank solution or MΦ-NPs exhibited no such features (Figure 4b). In particular, this suggested that the MΦ-NP itself, as a carrier for the *P. aeruginosa* antigens, had limited immunogenicity, which was expected given the murine origin of the membrane material. Similar results were also observed when looking at the axillary lymph node (Figure 4c,d).

The humoral immune response elicited by the MΦ-toxoids was further characterized by analyzing the production of antigen-specific antibody titers. Mice were subcutaneously vaccinated with the nanoformulation on day 0, followed by booster doses on day 7 and day 14 to further enhance titer production.[31] On day 21, which is approximately when immunoglobulin G (IgG) responses start to saturate,[31] the serum of each mouse was sampled, and the IgG titers against the antigenic material from PaS-1/2 were assayed by an indirect enzyme-linked immunosorbent assay (ELISA). From the data, it could be seen that vaccination with the MΦ-toxoids was able to significantly elevate anti-PaS titers above baseline levels (Figure 4e). As *P. aeruginosa* is a leading cause of nosocomial pneumonia,[49] the potential of MΦ-toxoid vaccination to protect against live bacterial infection was then evaluated using a murine model of pneumonia caused by a multidrug-resistant human clinical P4 isolate.[50] Following 3 subcutaneous vaccinations, each 1 week apart, mice were challenged intratracheally with the bacteria on day 35 to induce lung infection. At 24 h post-infection, the lungs were collected and subjected to various forms of analysis. A significant elevation of IgG titers was observed in the lung homogenate of vaccinated mice (Figure 4f), and this correlated with a marked decrease in bacterial load of approximately 2 orders of magnitude compared with control mice (Figure 4g). Histopathological analysis of the lungs reflected this large disparity in efficacy, as there was a significant reduction in congestion and acute inflammatory neutrophil infiltrate in the lung parenchyma of mice in the MΦ-toxoid-vaccinated group (Figure 4h).

A second set of immune response characterization studies involved the intranasal vaccination route, which has the potential to elicit systemic immune responses comparable to parenteral vaccination while concurrently generating mucosal immunity.[51] IgA antibodies are one of the main mediators of mucosal immune responses, and their presence in the nasal cavity or respiratory tract can act as a first line of defense against airborne pathogens.[52] After IgA class switching and maturation, IgA-producing B cells have been shown to migrate from nasal-associated lymphatic tissue to the cervical lymph nodes.[53] To assess the impact of MΦ-toxoid vaccination on this process, superficial cervical lymph node was collected 21 days after intranasal vaccination. Flow cytometric analysis showed that mice receiving the MΦ-toxoids had a significantly higher number of IgA-producing B cells compared with those receiving either blank solution or unloaded MΦ-NPs (Figure 5a). This finding was further corroborated by immunofluorescence staining of histological sections from the cervical lymph node (Figure 5b).

The humoral immune response generated by intranasal administration of the MΦ-toxoids was further studied by analyzing antibody production. Mice were intranasally vaccinated with the nanovaccine on day 0, along with boosters on day 7 and day 14. On day 21, both the serum and the bronchoalveolar lavage (BAL) fluid were sampled, and the antibody levels in each were assayed by indirect ELISAs. Within the BAL fluid, it was shown that the MΦ-

toxoids were capable of enhancing the production of both secretory IgA as well as IgG against PaS-1/2 (Figure 5c,d), indicating the successful generation of mucosal immunity that could be leveraged to inhibit bacterial lung infections. At the same time, significantly higher anti-PaS IgG levels were detected in the serum compared with the baseline established from the blank control group (Figure 5e), which indicated that the intranasal vaccination was potent enough to elicit strong systemic immunity. To evaluate protective efficacy, mice were intranasally vaccinated on the same schedule, followed by intratracheal bacteria challenge on day 35. Similar to the subcutaneous scenario, intranasal vaccination with the MΦ-toxoids resulted in significantly reduced bacteria counts within the lungs (Figure 5f), and this was also reflected in the lung histology (Figure 5g).

In conclusion, we have reported on the fabrication of a nanotoxoid formulation for use as a vaccine against gram-negative bacterial infections caused by *P. aeruginosa*. By employing a biomimetic toxin-detainment strategy using macrophage-mimicking nanoparticles, the resulting nanovaccine formulation was proven to be inherently multiantigenic and safe for *in vivo* administration given the ability of MΦ-NPs to neutralize both hemolytic and cytotoxic activity. When used to vaccinate mice, either by the subcutaneous or intranasal route, potent humoral immunity was generated, which significantly attenuated the severity of infection in a pneumonia model caused by live pathogenic *P. aeruginosa*. Of note, it was demonstrated that intranasal vaccination using the MΦ-toxoids could elicit both systemic immunity and mucosal immunity, which could have important implications for preventing a number of common infections, including those affecting the airways, gastrointestinal tract, urinary tract, and genitals. The extension of the nanotoxoid concept, where vaccines capable of generating multiantigenic immunity are fabricated through the broad function-based capture of toxic secretions, to gram-negative bacteria suggests that this approach is likely universal across the entire spectrum of pathogenic bacteria and could be used to overcome some of the challenges associated with traditional vaccination approaches. Unique formulations can be generated by changing the source of both the cell membrane coating and the bacterial antigens,[22] enabling the facile production of formulations custom-tailored to the needs of specific patient populations. In the future, more specific cell subsets, such as alveolar macrophages, could be explored as a membrane source to enhance antigen binding, and additional purification steps could be employed after nanotoxoid fabrication in order to improve vaccine specificity. Ultimately, the success of this platform could have a major impact on the clinical management of infectious disease by helping to address the challenging issue of antibiotic resistance.

Materials and Methods

MΦ-NP Fabrication.

Murine J774 cells (TIB-67, American Type Culture Collection) were maintained in Dulbecco's Modified Eagle Medium (Mediatech) supplemented with 10% fetal bovine serum (HyClone) and 1% penicillin–streptomycin (Gibco). The cells were harvested by directly scraping them off of the bottom of T-175 tissue culture flasks, and the cell membrane was derived by a combination of mechanical disruption and differential centrifugation using a previously reported method.[45] Polymeric nanoparticle cores were

synthesized by precipitating carboxyl-terminated poly(lactic-*co*-glycolic acid) (PLGA, 0.67 dL/g, 50:50 monomer ratio; LACTEL Absorbable Polymers) dissolved at 10 mg/mL in acetone into water, followed by evaporation under a vacuum to remove the organic solvent. To fabricate the final MΦ-NPs, the cell membrane was coated onto the preformed PLGA cores by mixing the two at a membrane protein to polymer weight ratio of 1:1, followed by sonication in a Fisher Scientific FS30D bath sonicator.

Preparation of Fractionated Bacterial Secretions.

The P4 *P. aeruginosa* clinical isolate, kindly provided by Dr. Victor Nizet,[50] was first streaked onto a Luria broth (LB; Sigma-Aldrich) agar plate and cultured overnight at 37 °C. A single colony was transferred into 5 mL of liquid LB for 24 h at 37 °C with shaking, and 1 mL was then transferred to another 100 mL of LB and cultured for another 24 h. The culture supernatant was collected after spinning down the bacteria at 5,000 *g* for 20 min. Saturated ammonium sulfate (Sigma-Aldrich) solution was added slowly to the supernatant up to a 75% volume ratio in a glass beaker while stirring at 4 °C. After stirring for 1 h, the solution was centrifuged at 3,000 *g* for 20 min and the pellet was collected. Solid ammonium sulfate was then added to the supernatant to obtain the equivalent of a 95% saturated solution volume ratio and stirred overnight before collecting a second pellet. Each pellet was dissolved in water, followed by desalting using a chromatography column prepared with fine G-25 Sephadex (GE Healthcare). During the desalting process, small volume fractions were collected, and the protein concentration of each was determined by a BCA protein assay (Pierce) per the manufacturer's instructions. For protein-containing fractions, hemolytic activity was assessed by adjusting each to 1× phosphate buffered saline (PBS) and incubating at 0.4 mg/mL with 2.5% RBCs collected from male CD-1 mice (Charles River Laboratories). After 30 min of incubation, the samples were spun down at 2,000 *g* for 5 min. Hemolysis was determined by measuring the absorbance of the supernatant at 540 nm using a Tecan Infinite M200 plate reader. A 100% lysis control was prepared by treating the RBCs with Triton X-100 (Sigma-Aldrich). Chromatography fractions from both pellets demonstrating considerable signal in the hemolysis assay were combined for further use as PaS-1. All the other protein-containing fractions were consolidated as PaS-2. All animal experiments were performed in accordance with National Institutes of Health guidelines and approved by the Institutional Animal Care and Use Committee of the University of California San Diego.

Neutralization of PaS Toxicity.

To assess the ability of MΦ-NPs to neutralize the biological activity of the PaS-1 fraction, 200 μg of the nanoparticles was incubated with either 20 μg or 40 μg of PaS-1 in water at 37 °C for 15 min, followed by adjustment to 1× PBS in a total volume of 100 μL. To test for hemolytic activity, an equal volume of 2.5% mouse RBCs was added, and the degree of hemolysis was measured after 30 min as described above. To test the impact of MΦ-NP preincubation on cytotoxic activity, J774 cells were plated into 96-well plates at a cell density of 6,000 cells per well. After allowing 24 h for attachment, the cells were incubated with PaS-1 at 20 μg/mL or 40 μg/mL and MΦ-NP at 200 μg/mL for 72 h. Cell viability was assayed using an MTS cell proliferation assay (Promega) following the manufacturer's instructions. Untreated cells were used as the 100% viability control. For both studies,

equivalent amounts of PaS-1 only or MΦ-NPs only were used for comparison. The impact of nanoparticle preincubation on the cytotoxic activity of the PaS-2 fraction was tested in a similar manner, with 200 μg/mL of the MΦ-NPs incubated with either 1 μg/mL or 4 μg/mL of PaS-2. Lack of hemolytic activity was evaluated by incubating with RBCs at a final PaS-2 protein concentration of 200 μg/mL.

MΦ-Toxoid Formulation and Characterization.

The final MΦ-toxoids were fabricated by incubating 200 μg of MΦ-NPs with 40 μg of PaS-1 and 1 μg of PaS-2 at 37 °C for 15 min, and this formulation was used to carry out all subsequent studies. The size and surface zeta potential of the nanoformulations was measured by dynamic light scattering using a Malvern ZEN 3600 Zetasizer. The structure of the nanovaccine was examined after negative staining with 1 wt% uranyl acetate (Electron Microscopy Sciences) on a carbon-coated 400-mesh copper grid (Electron Microscopy Sciences) using a Tecnai Spirit transmission electron microscope. Stability of the MΦ-toxoids was evaluated by suspending the nanoparticles at a concentration of 1 mg/mL in 10% sucrose and measuring size over the course of 1 week. Multiplexed, tandem mass tag-based quantitative proteomic analysis of the MΦ-toxoids was carried out on an Orbitrap Fusion using a previously reported method.[39] The prepared samples were run on an in-house column packed with 5 μm C4 resin, 3 μm C18 resin, and 1.8 μm C18 resin (Sepax) of lengths 0.5 cm, 0.5 cm, and 29 cm, respectively, using a three-hour gradient ranging from 3% to 100% acetonitrile in 0.125% formic acid. Following data acquisition and quantitation, spectra were searched against the PAO1 *P. aeruginosa* reference proteome database (Uniprot, 10/1/2018) and the *Mus musculus* reference proteome (Uniprot, 7/2/2018) using Proteome Discoverer 2.0 software (Thermo Scientific). Details of the analysis and data normalization procedure are elucidated in great detail in a previously published study.[39] Proteins were determined to be differentially abundant in volcano plots by π score, which is a metric that considers both fold-change and p-value-based significance.[40] Raw spectral data are available at ProteomXchange under the identifier PXD013108.

Safety Studies.

To study *in vitro* safety, the hemolytic and cytotoxic activity of the MΦ-toxoid formulation were assessed. Blank solution (10% sucrose), PaS-1/2 (40 μg PaS-1 + 1 μg PaS-2), MΦ-NPs (200 μg), or MΦ-toxoids (200 μg MΦ-NP preincubated with 40 μg PaS-1 + 1 μg PaS-2) were incubated with mouse RBCs or J774 macrophages, and the corresponding assays were carried out as described above. To evaluate *in vivo* safety, 200 μL of blank solution (10% sucrose), PaS-1/2 (300 μg PaS-1 + 7.5 μg PaS-2), MΦ-NPs (1.5 mg), or MΦ-toxoids (1.5 mg MΦ-NP preincubated with 300 μg PaS-1 + 7.5 μg PaS-2) were subcutaneously injected into the neck region of male CD-1 mice. After 48 h, the mice were euthanized, and skin samples were collected for histological processing. Sections were stained with hematoxylin and eosin using SelecTech reagents (Leica Biosystems). Brightfield images were acquired using a Keyence BZ-9000 microscope.

Immune Response to Subcutaneous Vaccination.

Six-week-old male CD-1 mice were subcutaneously administered with 200 μL of blank solution (10% sucrose), MΦ-NPs (1.5 mg), or MΦ-toxoids (1.5 mg MΦ-NP preincubated

with 300 μg PaS-1 + 7.5 μg PaS-2) in the neck region. On day 21 after immunization, the superficial cervical lymph nodes and axillary lymph nodes were collected for analysis. For immunohistochemistry, the lymph nodes were cryosectioned and stained with Pacific Blue-labeled anti-mouse/human B220 (RA3–6B2; Biolegend), Alexa488-labeled anti-mouse IgD (11–26c.2a; Biolegend), and Alexa647-labeled anti-mouse/human GL-7 (GL7; Biolegend). Fluorescence imaging was conducted on a Keyence BZ-9000 microscope. For flow cytometric analysis, the lymph nodes were dissociated into single cell suspensions using 1 mg/mL collagenase D (Roche) and 1 mg/mL DNAse I (Roche). The cells were then stained with the above antibodies, followed by data collection on a Becton Dickinson FACSCanto-II flow cytometer. Analysis was performed using Flowjo software.

To study the antibody responses, six-week-old male CD-1 mice were subcutaneously administered with 200 μL of blank solution (10% sucrose) or MΦ-toxoids (1.5 mg MΦ-NP preincubated with 300 μg PaS-1 + 7.5 μg PaS-2) in the neck region on days 0, 7, and 14. On day 21, the blood from each mouse was sampled, and the serum was subsequently derived by centrifugation at 700 *g* for 5 min. On day 35, the mice were intratracheally challenged with 40 μL of 1×10^6 colony forming units (CFU) of *P. aeruginosa*, and the lungs were collected and homogenized 24 h post-challenge. Titers for antigen-specific IgG in the blood serum and lung homogenate were assessed by an indirect ELISA using plates coated with PaS-1/2 following a previously reported protocol.[32]

Immune Response to Intranasal Vaccination.

Six-week-old male CD-1 mice were intranasally administered with 20 μL of blank solution (10% sucrose), MΦ-NPs (0.75 mg), or MΦ-toxoids (0.75 mg MΦ-NP preincubated with 150 μg PaS-1 + 3.75 μg PaS-2). On day 21 after immunization, the superficial cervical lymph nodes were collected for analysis. For immunohistochemistry, the lymph nodes were cryosectioned and stained with Pacific Blue-labeled anti-mouse/human B220 and FITC-labeled anti-mouse IgA (11-44-2; SouthernBiotech). Fluorescence images were obtained using a Keyence BZ-9000 microscope. For flow cytometric analysis, the lymph nodes were dissociated into single cell suspensions and stained with the above antibodies followed by data collection on a Becton Dickinson FACSCanto-II flow cytometer. Analysis was performed using Flowjo software.

To study the antibody responses, six-week-old male CD-1 mice were intranasally vaccinated with 20 μL of blank solution (10% sucrose) or MΦ-toxoids (0.75 mg MΦ-NP preincubated with 150 μg PaS-1 + 3.75 μg PaS-2) on days 0, 7, and 14. On day 21, the serum from each mouse was sampled to assess for the presence of systemic antigen-specific IgG titers. BAL fluid was also obtained to determine the relative levels of antigen-specific mucosal sIgA and IgG by indirect ELISAs using plates coated with PaS-1/2.

Protective Efficacy against P. aeruginosa Infection.

Six-week-old male CD-1 mice were immunized either subcutaneously or intranasally on days 0, 7, and 14 using the corresponding dosages from the immune response studies above. On day 35 after the first administration, the mice were anesthetized using a cocktail of 150 mg/kg ketamine (Zoetis) and 10 mg/kg xylazine (Lloyd Laboratories), followed by

intratracheal challenge with 40 μL of 1×10^6 CFU of *P. aeruginosa*. The mice were euthanized 24 h after bacteria inoculation and the lungs were collected and processed for bacterial enumeration following a previously published protocol.[32] In a different set of mice subjected to the same vaccinations and bacterial challenge, the lung tissues were collected 24 h post-infection, embedded in paraffin, sectioned, and stained with hematoxylin and eosin. Brightfield images were acquired using a Keyence BZ-9000 microscope.

Supplementary Material

Refer to Web version on PubMed Central for supplementary material.

ACKNOWLEDGMENTS

This work was supported by the Defense Threat Reduction Agency Joint Science and Technology Office for Chemical and Biological Defense under Grant Number HDTRA1–18-1-0014. J.Z. was supported by a National Institutes of Health 5T32CA153915 training grant from the National Cancer Institute.

REFERENCES

(1). Zaman SB; Hussain MA; Nye R; Mehta V; Mamun KT; Hossain N, A Review on Antibiotic Resistance: Alarm Bells are Ringing. Cureus 2017, 9, e1403. [PubMed: 28852600]

(2). Cosgrove SE, The Relationship between Antimicrobial Resistance and Patient Outcomes: Mortality, Length of Hospital Stay, and Health Care Costs. Clin. Infect. Dis 2006, 42, S82–S89. [PubMed: 16355321]

(3). Sadikot RT; Blackwell TS; Christman JW; Prince AS, Pathogen-Host Interactions in *Pseudomonas aeruginosa* Pneumonia. Am. J. Respir. Crit. Care Med 2005, 171, 1209–1223. [PubMed: 15695491]

(4). Lister PD; Wolter DJ; Hanson ND, Antibacterial-Resistant *Pseudomonas* aeruginosa: Clinical Impact and Complex Regulation of Chromosomally Encoded Resistance Mechanisms. Clin. Microbiol. Rev 2009, 22, 582–610. [PubMed: 19822890]

(5). Henrichfreise B; Wiegand I; Pfister W; Wiedemann B, Resistance Mechanisms of Multiresistant *Pseudomonas aeruginosa* Strains from Germany and Correlation with Hypermutation. Antimicrob. Agents Chemother 2007, 51, 4062–4070. [PubMed: 17876002]

(6). Lambert PA, Mechanisms of Antibiotic Resistance in Pseudomonas aeruginosa. J. R. Soc. Med 2002, 95, 22–26. [PubMed: 12216271]

(7). Willyard C, The Drug-Resistant Bacteria that Pose the Greatest Health Threats. Nature 2017, 543, 15. [PubMed: 28252092]

(8). Hurley MN; Camara M; Smyth AR, Novel Approaches to the Treatment of *Pseudomonas aeruginosa* Infections in Cystic Fibrosis. Eur. Respir. J 2012, 40, 1014–1023. [PubMed: 22743672]

(9). Smith WD; Bardin E; Cameron L; Edmondson CL; Farrant KV; Martin I; Murphy RA; Soren O; Turnbull AR; Wierre-Gore N; Alton EW; Bundy JG; Bush A; Connett GJ; Faust SN; Filloux A; Freemont PS; Jones AL; Takats Z; Webb JS, et al., Current and Future Therapies for *Pseudomonas aeruginosa* Infection in Patients with Cystic Fibrosis. FEMS Microbiol. Lett 2017, 364, fnx121.

(10). Mendoza N; Ravanfar P; Satyaprakash A; Pillai S; Creed R, Existing Antibacterial Vaccines. Dermatol. Ther 2009, 22, 129–142. [PubMed: 19335724]

(11). Kaufmann SH, The Contribution of Immunology to the Rational Design of Novel Antibacterial Vaccines. Nat. Rev. Microbiol 2007, 5, 491–504. [PubMed: 17558425]

(12). Merakou C; Schaefers MM; Priebe GP, Progress toward the Elusive *Pseudomonas aeruginosa* Vaccine. Surg. Infect. (Larchmt) 2018, 19, 757–768. [PubMed: 30388058]

(13). Priebe GP; Goldberg JB, Vaccines for Pseudomonas aeruginosa: A Long and Winding Road. Expert Rev. Vaccines 2014, 13, 507–519. [PubMed: 24575895]

(14). Muhlen S; Dersch P, Anti-Virulence Strategies to Target Bacterial Infections. Curr. Top. Microbiol. Immunol 2016, 398, 147–183. [PubMed: 26942418]

(15). Cegelski L; Marshall GR; Eldridge GR; Hultgren SJ, The Biology and Future Prospects of Antivirulence Therapies. Nat. Rev. Microbiol 2008, 6, 17–27. [PubMed: 18079741]

(16). Totsika M, Disarming Pathogens: Benefits and Challenges of Antimicrobials that Target Bacterial Virulence Instead of Growth and Viability. Future Med. Chem 2017, 9, 267–269. [PubMed: 28207349]

(17). Mellbye B; Schuster M, The Sociomicrobiology of Antivirulence Drug Resistance: A Proof of Concept. MBio 2011, 2, e00131–11. [PubMed: 21990612]

(18). Gellatly SL; Hancock REW, Pseudomonas aeruginosa: New Insights into Pathogenesis and Host Defenses. Pathog. Dis 2013, 67, 159–173. [PubMed: 23620179]

(19). Strateva T; Mitov I, Contribution of an Arsenal of Virulence Factors to Pathogenesis of Pseudomonas aeruginosa Infections. Ann. Microbiol 2011, 61, 717–732.

(20). Hauser AR, Pseudomonas aeruginosa: So Many Virulence Factors, So Little Time. Crit. Care Med 2011, 39, 2193–2194. [PubMed: 21849835]

(21). Bakour S; Sankar SA; Rathored J; Biagini P; Raoult D; Fournier PE, Identification of Virulence Factors and Antibiotic Resistance Markers using Bacterial Genomics. Future Microbiol. 2016, 11, 455–466. [PubMed: 26974504]

(22). Fang RH; Kroll AV; Gao W; Zhang L, Cell Membrane Coating Nanotechnology. Adv. Mater 2018, 30, 1706759.

(23). Fang RH; Jiang Y; Fang JC; Zhang L, Cell Membrane-Derived Nanomaterials for Biomedical Applications. Biomaterials 2017, 128, 69–83. [PubMed: 28292726]

(24). Hu CM; Zhang L; Aryal S; Cheung C; Fang RH; Zhang L, Erythrocyte Membrane-Camouflaged Polymeric Nanoparticles as a Biomimetic Delivery Platform. Proc. Natl. Acad. Sci. USA 2011, 108, 10980–10985. [PubMed: 21690347]

(25). Hu CM; Fang RH; Wang KC; Luk BT; Thamphiwatana S; Dehaini D; Nguyen P; Angsantikul P; Wen CH; Kroll AV; Carpenter C; Ramesh M; Qu V; Patel SH; Zhu J; Shi W; Hofman FM; Chen TC; Gao W; Zhang K, et al., Nanoparticle Biointerfacing by Platelet Membrane Cloaking. Nature 2015, 526, 118–121. [PubMed: 26374997]

(26). Fang RH; Hu CM; Luk BT; Gao W; Copp JA; Tai Y; O'Connor DE; Zhang L, Cancer Cell Membrane-Coated Nanoparticles for Anticancer Vaccination and Drug Delivery. Nano. Lett 2014, 14, 2181–2188. [PubMed: 24673373]

(27). Chen Y; Chen M; Zhang Y; Lee JH; Escajadillo T; Gong H; Fang RH; Gao W; Nizet V; Zhang L, Broad-Spectrum Neutralization of Pore-Forming Toxins with Human Erythrocyte Membrane-Coated Nanosponges. Adv. Healthc. Mater 2018, 7, 1701366.

(28). Thamphiwatana S; Angsantikul P; Escajadillo T; Zhang Q; Olson J; Luk BT; Zhang S; Fang RH; Gao W; Nizet V; Zhang L, Macrophage-Like Nanoparticles Concurrently Absorbing Endotoxins and Proinflammatory Cytokines for Sepsis Management. Proc. Natl. Acad. Sci. USA 2017, 114, 11488–11493. [PubMed: 29073076]

(29). Fang RH; Luk BT; Hu CM; Zhang L, Engineered Nanoparticles Mimicking Cell Membranes for Toxin Neutralization. Adv. Drug Deliv. Rev 2015, 90, 69–80. [PubMed: 25868452]

(30). Hu CM; Fang RH; Copp J; Luk BT; Zhang L, A Biomimetic Nanosponge that Absorbs Pore-Forming Toxins. Nat. Nanotechnol 2013, 8, 336–340. [PubMed: 23584215]

(31). Hu CM; Fang RH; Luk BT; Zhang L, Nanoparticle-Detained Toxins for Safe and Effective Vaccination. Nat. Nanotechnol 2013, 8, 933–938. [PubMed: 24292514]

(32). Wang F; Fang RH; Luk BT; Hu CJ; Thamphiwatana S; Dehaini D; Angsantikul P; Kroll AV; Pang Z; Gao W; Lu W; Zhang L, Nanoparticle-Based Antivirulence Vaccine for the Management of Methicillin-Resistant *Staphylococcus aureus* Skin Infection. Adv. Funct. Mater 2016, 26, 1628–1635. [PubMed: 27325913]

(33). Wei X; Gao J; Wang F; Ying M; Angsantikul P; Kroll AV; Zhou J; Gao W; Lu W; Fang RH; Zhang L, *In Situ* Capture of Bacterial Toxins for Antivirulence Vaccination. Adv. Mater 2017, 29, 1701644.

(34). Zhang L; Wang CC, Inflammatory Response of Macrophages in Infection. Hepatobiliary Pancreat. Dis. Int 2014, 13, 138–152. [PubMed: 24686541]

(35). Aderem A, Phagocytosis and the Inflammatory Response. J. Infect. Dis 2003, 187, S340–S345. [PubMed: 12792849]

(36). Sawyer JG; Martin NL; Hancock RE, Interaction of Macrophage Cationic Proteins with the Outer Membrane of *Pseudomonas aeruginosa*. Infect. Immun 1988, 56, 693–698. [PubMed: 3125111]

(37). Mahenthiralingam E; Speert DP, Nonopsonic Phagocytosis of *Pseudomonas aeruginosa* by Macrophages and Polymorphonuclear Leukocytes Requires the Presence of the Bacterial Flagellum. Infect. Immun 1995, 63, 4519–4523. [PubMed: 7591095]

(38). Basso P; Ragno M; Elsen S; Reboud E; Golovkine G; Bouillot S; Huber P; Lory S; Faudry E; Attree I, *Pseudomonas aeruginosa* Pore-Forming Exolysin and Type IV Pili Cooperate to Induce Host Cell Lysis. MBio 2017, 8, e02250–16. [PubMed: 28119472]

(39). Lapek JD Jr.; Fang RH; Wei X; Li P; Wang B; Zhang L; Gonzalez DJ, Biomimetic Virulomics for Capture and Identification of Cell-Type Specific Effector Proteins. ACS Nano 2017, 11, 11831–11838. [PubMed: 28892626]

(40). Xiao Y; Hsiao TH; Suresh U; Chen HI; Wu X; Wolf SE; Chen Y, A Novel Significance Score for Gene Selection and Ranking. Bioinformatics 2014, 30, 801–807. [PubMed: 22321699]

(41). Feldman M; Bryan R; Rajan S; Scheffler L; Brunnert S; Tang H; Prince A, Role of Flagella in Pathogenesis of *Pseudomonas aeruginosa* Pulmonary Infection. Infect. Immun 1998, 66, 43–51. [PubMed: 9423837]

(42). Saha S; Takeshita F; Matsuda T; Jounai N; Kobiyama K; Matsumoto T; Sasaki S; Yoshida A; Xin KQ; Klinman DM; Uematsu S; Ishii KJ; Akira S; Okuda K, Blocking of the TLR5 Activation Domain Hampers Protective Potential of Flagellin DNA Vaccine. J. Immunol 2007, 179, 1147–1154. [PubMed: 17617608]

(43). Raoust E; Balloy V; Garcia-Verdugo I; Touqui L; Ramphal R; Chignard M, Pseudomonas aeruginosa LPS or Flagellin are Sufficient to Activate TLR-Dependent Signaling in Murine Alveolar Macrophages and Airway Epithelial Cells. PLoS ONE 2009, 4, e7259. [PubMed: 19806220]

(44). Weimer ET; Lu H; Kock ND; Wozniak DJ; Mizel SB, A Fusion Protein Vaccine Containing OprF Epitope 8, OprI, and Type A and B Flagellins Promotes Enhanced Clearance of Nonmucoid *Pseudomonas aeruginosa*. Infect. Immun 2009, 77, 2356–2366. [PubMed: 19349426]

(45). Kroll AV; Fang RH; Jiang Y; Zhou J; Wei X; Yu CL; Gao J; Luk BT; Dehaini D; Gao W; Zhang L, Nanoparticulate Delivery of Cancer Cell Membrane Elicits Multiantigenic Antitumor Immunity. Adv. Mater 2017, 29, 1703969.

(46). De Silva NS; Klein U, Dynamics of B Cells in Germinal Centres. Nat. Rev. Immunol 2015, 15, 137–148. [PubMed: 25656706]

(47). Priebe GP; Walsh RL; Cederroth TA; Kamei A; Coutinho-Sledge YS; Goldberg JB; Pier GB, IL-17 is a Critical Component of Vaccine-Induced Protection against Lung Infection by Lipopolysaccharide-Heterologous Strains of *Pseudomonas aeruginosa*. J. Immunol 2008, 181, 4965–4975. [PubMed: 18802100]

(48). Moser C; Jensen PO; Kobayashi O; Hougen HP; Song Z; Rygaard J; Kharazmi A; N, H. b., Improved Outcome of Chronic *Pseudomonas aeruginosa* Lung Infection is Associated with Induction of a Th1-Dominated Cytokine Response. Clin. Exp. Immunol 2002, 127, 206–213. [PubMed: 11876741]

(49). Gaynes R; Edwards JR; National Nosocomial Infections Surveillance, S., Overview of Nosocomial Infections Caused by Gram-Negative Bacilli. Clin. Infect. Dis 2005, 41, 848–854. [PubMed: 16107985]

(50). Lin L; Nonejuie P; Munguia J; Hollands A; Olson J; Dam Q; Kumaraswamy M; Rivera H Jr.; Corriden R; Rohde M; Hensler ME; Burkart MD; Pogliano J; Sakoulas G; Nizet V, Azithromycin Synergizes with Cationic Antimicrobial Peptides to Exert Bactericidal and Therapeutic Activity against Highly Multidrug-Resistant Gram-Negative Bacterial Pathogens. EBioMedicine 2015, 2, 690–698. [PubMed: 26288841]

(51). Zhang L; Wang W; Wang S, Effect of Vaccine Administration Modality on Immunogenicity and Efficacy. Expert Rev. Vaccines 2015, 14, 1509–1523. [PubMed: 26313239]

(52). Woof JM; Kerr MA, The Function of Immunoglobulin A in Immunity. J. Pathol 2006, 208, 270–282. [PubMed: 16362985]

(53). Kiyono H; Fukuyama S, NALT- *Versus* Peyer's-Patch-Mediated Mucosal Immunity. Nat. Rev. Immunol 2004, 4, 699–710. [PubMed: 15343369]

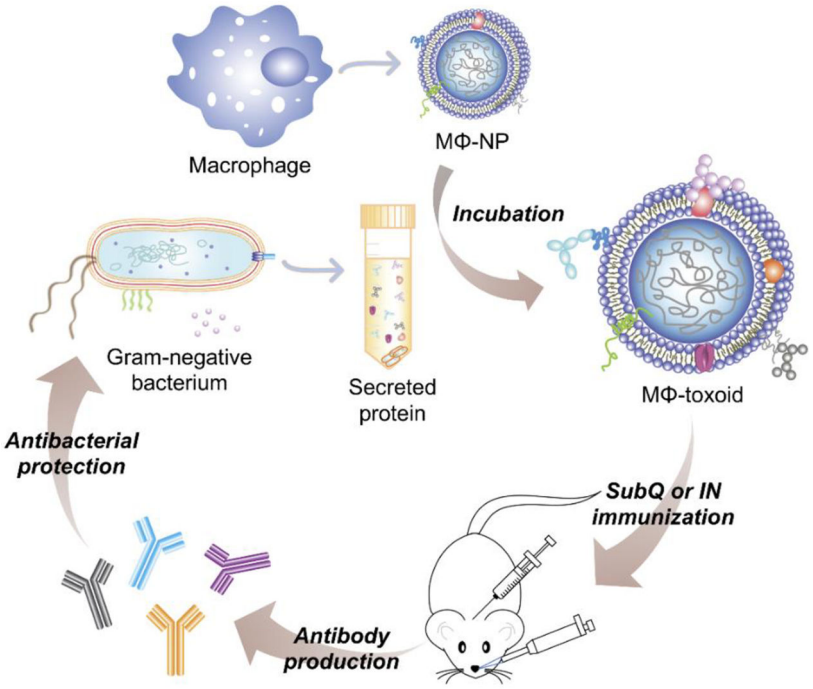

Figure 1.

Schematic illustration of multiantigenic nanotoxoids against gram-negative bacterial infection. Macrophage-mimicking nanoparticles (MΦ-NPs) are fabricated by coating the plasma membrane of macrophages onto polymeric nanoparticle cores. These particles can then be used in the generation of multiantigenic nanotoxoids through the capture and neutralization of secretions from gram-negative bacteria. When vaccinated either by the subcutaneous (subQ) or intranasal (IN) route, mice receiving macrophage nanotoxoids (MΦ-toxoids) generate potent antibacterial immunity that can be used to protect against subsequent bacterial challenge.

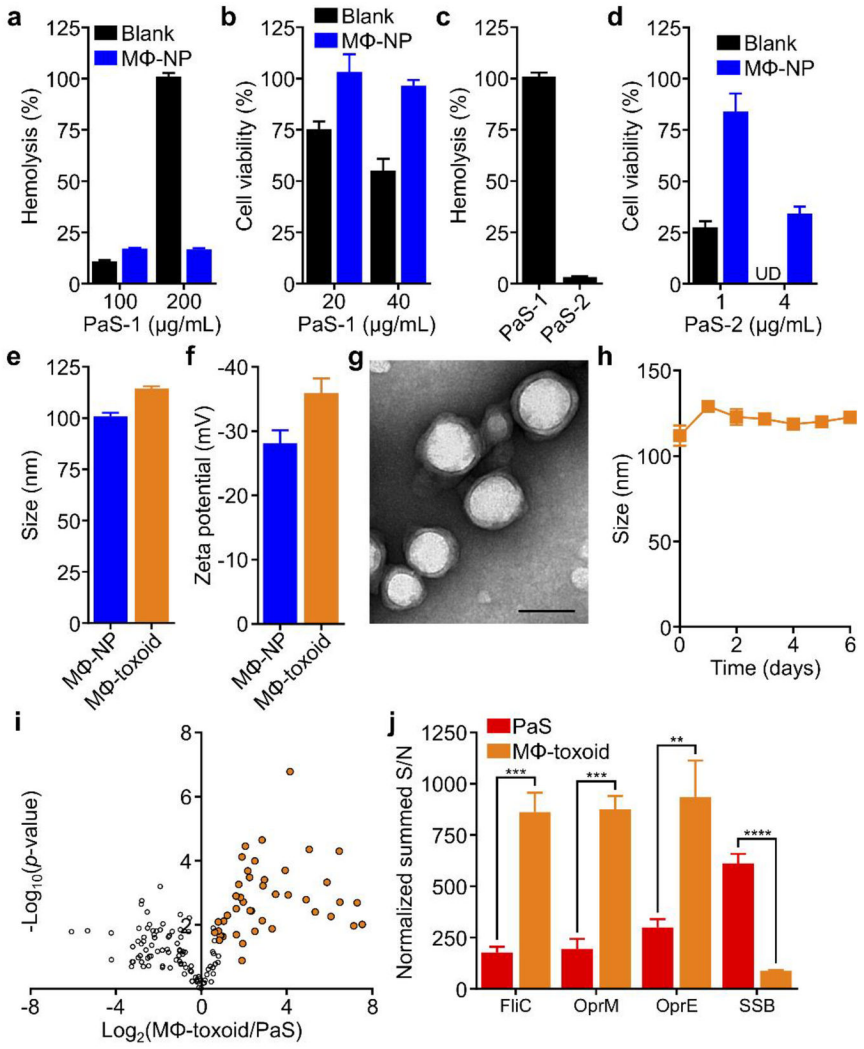

Figure 2.

MΦ-toxoid formulation and characterization. (a) Hemolysis of RBCs when incubated with 100 or 200 μg/mL of PaS-1 in the absence or presence of MΦ-NPs (n = 3; mean + SD). (b) Cell viability of J774 macrophages after 72 h of incubation with 20 or 40 μg/mL of PaS-1 in the absence or presence of MΦ-NPs (n = 3; mean + SD). (c) Hemolysis of RBCs when incubated with 200 μg/mL of PaS-1 or PaS-2 (n = 3; mean + SD). (d) Cell viability of J774 macrophages after 72 h of incubation with 1 or 4 μg/mL of PaS-2 in the absence or presence of MΦ-NPs (n = 3; mean + SD; UD: undetectable). (e) Size of MΦ-NPs and MΦ-toxoids (n = 3; mean + SD). (f) Zeta potential of MΦ-NPs and MΦ-toxoids (n = 3; mean + SD). (g) Transmission electron microscope (TEM) image of MΦ-toxoids negatively stained with uranyl acetate (scale bar: 100 nm). (h) Size (diameter, nm) of MΦ-toxoids over time (n = 3; mean ± SD). (i) Visualization of individual *P. aeruginosa* proteins on MΦ-toxoids based on fold-enrichment over PaS-1/2 and p-values calculated from proteomic analysis (orange dots: π > 1.1082). (j) Summed signal-to-noise (S/N) values for selected *P. aeruginosa* proteins enriched on MΦ-toxoids, including flagellin (FliC), OprM, and OprE, as well as a negatively

enriched protein, single-stranded DNA-binding protein (SSB) ($n = 3$; mean + SD; $^{**}p < 0.01$, $^{***}p < 0.001$, $^{****}p < 0.0001$, Student's t-test).

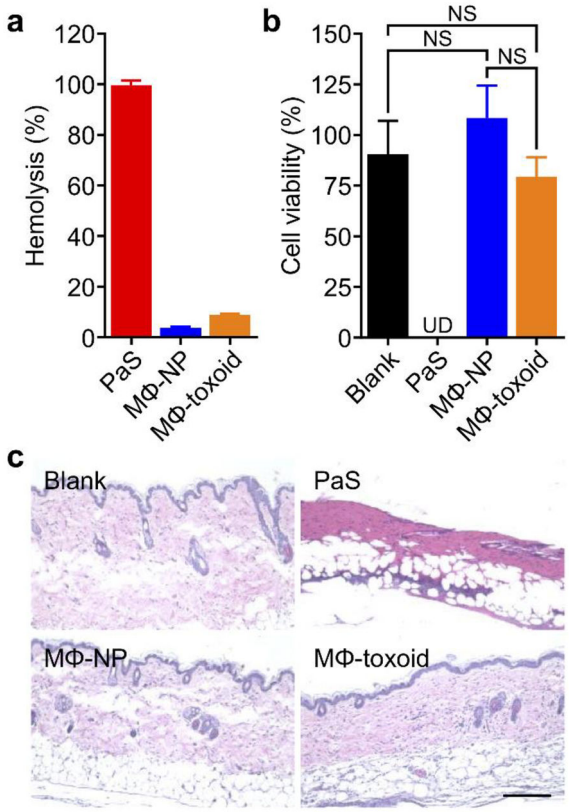

Figure 3.

MΦ-toxoid safety evaluation. (a) Hemolysis of RBCs when incubated with PaS-1/2, MΦ-NPs, or MΦ-toxoids ($n = 3$; mean + SD). (b) Cell viability of J774 macrophages after 72 h of incubation with blank solution, PaS-1/2, MΦ-NPs, or MΦ-toxoids ($n = 3$; mean + SD; NS: not significant, one-way ANOVA; UD: undetectable). (c) Hematoxylin and eosin (H&E)-stained histological sections of skin samples collected from mice 48 h after subcutaneous injection of blank solution, PaS-1/2, MΦ-NPs, or MΦ-toxoids (scale bar: 200 μm).

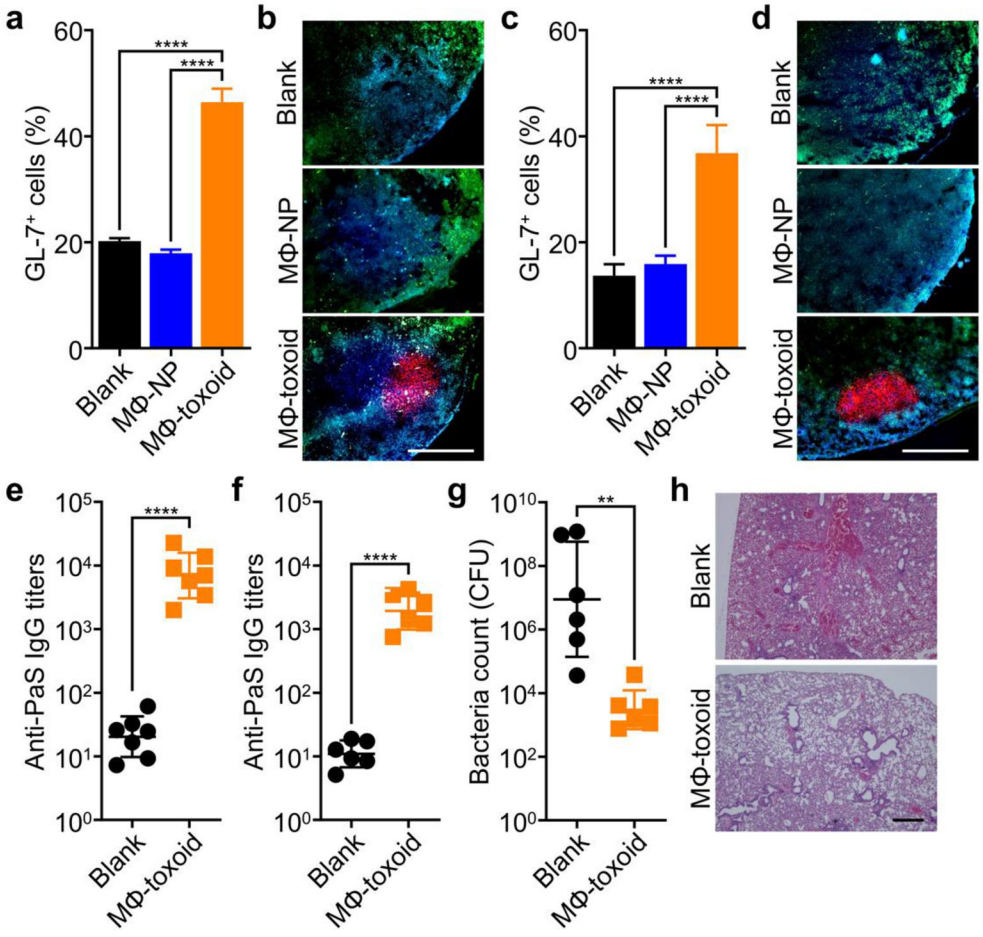

Figure 4.

Immune response to subcutaneous MΦ-toxoid immunization. (a) Proportion of $B220^{+}IgD^{low}$ B cells in the superficial cervical lymph node with the GL-7^{+} germinal center phenotype 21 days after subcutaneous administration with blank solution, MΦ-NPs, or MΦ-toxoids ($n = 3$; mean + SD; ****$p < 0.0001$, one-way ANOVA). (b) Histological sections of the superficial cervical lymph node from mice vaccinated as in (a) (blue: B220, green: IgD, red: GL-7; scale bar: 200 μm). (c) Proportion of $B220^{+}IgD^{low}$ B cells in the axillary lymph node with the GL-7^{+} germinal center phenotype 21 days after subcutaneous administration with blank solution, MΦ-NPs, or MΦ-toxoids ($n = 3$; mean + SD; ****$p < 0.0001$, one-way ANOVA). (d) Histological sections of the axillary lymph node from mice vaccinated as in (c) (blue: B220, green: IgD, red: GL-7; scale bar: 200 μm). (e) Anti-PaS IgG titers in the serum of mice on day 21 following vaccinations on days 0, 7, and 14 with blank solution or MΦ-toxoids ($n = 7$; geometric mean ± SD; ****$p < 0.0001$, Student's t-test). (f) Anti-PaS titers in the lungs of mice 24 h after intratracheal *P. aeruginosa* challenge on day 35 following subcutaneous vaccinations on days 0, 7, and 14 with blank solution or MΦ-toxoids ($n = 6$; geometric mean ± SD; ****$p < 0.0001$, Student's t-test). (g) Bacterial load in the lungs of mice vaccinated and infected as in (f) ($n = 6$; geometric mean ± SD; **$p < 0.01$, Student's t-test). (h) H&E-stained histological sections of lungs collected from mice vaccinated and infected as in (f) (scale bar: 500 μm).

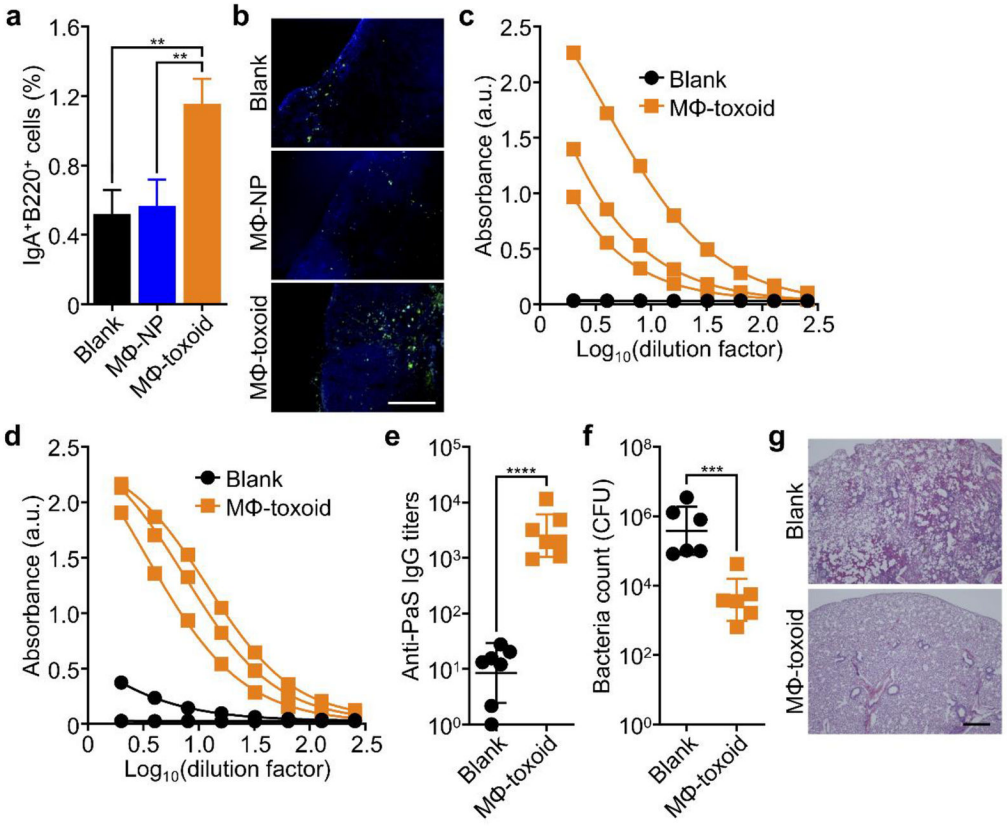

Figure 5.

Immune response to intranasal MΦ-toxoid immunization. (a) Proportion of IgA-producing B cells (IgA^+B220^+ phenotype) in the superficial cervical lymph node 21 days after intranasal administration with blank solution, MΦ-NPs, or MΦ-toxoids ($n = 3$; mean + SD; $^{**}p < 0.01$, one-way ANOVA). (b) Histological sections of the superficial cervical lymph node from mice vaccinated as in (a) (blue: B220, green: IgA; scale bar: 200 μm). (c,d) Absorbance plots from ELISAs probing for anti-PaS secretory IgA (sIgA, c) and IgG (d) levels in the BAL fluid of mice on day 21 following intranasal vaccinations on days 0, 7, and 14 with blank solution or MΦ-toxoids ($n = 3$). (e) Anti-PaS IgG titers in the serum of mice on day 21 following intranasal vaccinations on days 0, 7, and 14 with blank solution or MΦ-toxoids ($n = 7$; geometric mean ± SD; $^{****}p < 0.0001$, Student's *t*-test). (f) Bacterial load in the lungs of mice 24 h after intratracheal *P. aeruginosa* challenge on day 35 following intranasal vaccinations on days 0, 7, and 14 with blank solution or MΦ-toxoids ($n = 6$; geometric mean ± SD; $^{***}p < 0.001$, Student's *t*-test). (g) H&E-stained histological sections of lungs from mice vaccinated and infected as in (f) (scale bar: 500 μm).